HHS Public Access

Author manuscript

ACS Biomater Sci Eng. Author manuscript; available in PMC 2017 December 14.

Published in final edited form as:

ACS Biomater Sci Eng. 2017 June 12; 3(6): 1051–1061. doi:10.1021/acsbiomaterials.6b00814.

Glucose-Stimulated Insulin Response of Silicon Nanopore-Immunoprotected Islets under Convective Transport

Shang Song[†], **Raymond Yeung**[†], **Jaehyun Park**[†], **Andrew M Posselt**[‡], **Tejal A Desai**[†], **Qizhi Tang**[‡], and **Shuvo Roy**[*,†]

[†]Department of Bioengineering and Therapeutic Sciences, University of California–San Francisco, San Francisco, California 94158, United States

[‡]Department of Surgery, University of California–San Francisco, San Francisco, California 94143, United States

Abstract

Major clinical challenges associated with islet transplantation for type 1 diabetes include shortage of donor organs, poor engraftment due to ischemia, and need for immunosuppressive medications. Semipermeable membrane capsules can immunoprotect transplanted islets by blocking passage of the host's immune components while providing exchange of glucose, insulin, and other small molecules. However, capsules-based diffusive transport often exacerbates ischemic injury to islets by reducing the rate of oxygen and nutrient transport. We previously reported the efficacy of a newly developed semipermeable ultrafiltration membrane, the silicon nanopore membrane (SNM) under convective-driven transport, in limiting the passage of pro-inflammatory cytokines while overcoming the mass transfer limitations associated with diffusion through nanometer-scale pores. In this study, we report that SNM-encapsulated mouse islets perfused in culture solution under convection outperformed those under diffusive conditions in terms of magnitude (1.49-fold increase in stimulation index and 3.86-fold decrease in shutdown index) and rate of insulin secretion (1.19-fold increase and 6.45-fold decrease during high and low glucose challenges), respectively. Moreover, SNM-encapsulated mouse islets under convection demonstrated rapid glucose—insulin sensing within a physiologically relevant time-scale while retaining healthy islet viability even under cytokine exposure. We conclude that encapsulation of islets with SNM under convection improves islet in vitro functionality. This approach may provide a novel strategy for islet transplantation in the clinical setting.

Graphical abstract

[*]**Corresponding Author:** shuvo.roy@ucsf.edu. Phone: 415-514-9666. Fax: 415-514-9766.

Supporting Information

The Supporting Information is available free of charge on the ACS Publications website at DOI: 10.1021/acsbiomaterials.6b00814. Glucose-stimulated insulin kinetics and viability of membrane-encapsulated mouse islets under convection and diffusion with or without cytokine exposure (SμM, Conv & Diff vs SNM, Diff) (PDF)

ORCID

Shang Song: 0000-0002-8637-5086

Raymond Yeung: 0000-0002-1020-1928

Notes

The authors declare the following competing financial interest(s): Dr. Shuvo Roy is a co-founder of Silicon Kidney, LLC. There are no competing interests or conflicts of interest related to the work presented in this manuscript for all authors.

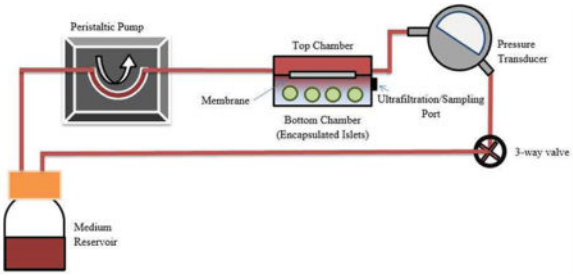

Keywords

silicon nanopore membranes (SNM); convection; immunoisolation; glucose-insulin kinetics; diffusion

1. INTRODUCTION

Type 1 diabetes (T1D) is an autoimmune disease that results in destruction of the insulin-producing β-cells within the pancreatic islets of Langerhans. Islet transplantation offers a promising way to treat T1D by directly infusing cadaveric islets into the portal vein of the recipient's liver.[1] The transplanted islets engraft and produce insulin in response to serum glucose levels. However, primary challenges affecting islet graft survival are donor availability, poor engraftment, and compounded immune response to the transplant in addition to adverse side effects from life-long immunosuppression.[2–5] Cell encapsulation with a selective, semipermeable membrane provides an attractive means to protect islets from immune damage while allowing the exchange of nutrients and small molecules.[6] Previous studies have showed that large antibodies (IgM: 950 000 Da) and complement (C1q: 410 000 Da) were blocked by a membrane with a maximum pore diameter of 30 nm.[7,8] However, pro-inflammatory cytokines including tumor necrosis factor-alpha (TNF-α) (17 300 Da; Stokes diameter, 3.80 nm), interferon-gamma (IFN-γ) (15 600 Da; Stokes diameter, 3.67 nm), and interlukin-1 beta (IL-1β) (17 500 Da; Stokes diameter: 3.81 nm) that are known to synergistically induce cytotoxic effects on islets are much smaller in size and are more challenging to exclude.[5,8,9] Although a nominal pore size on the scale of nanometers is advantageous for creating an immunoprotective environment,[7,8,10] solutes diffuse slower through the pores as their sizes approach the critical geometric dimension of the pores.[11] The slow diffusion and resulting impact on mass transport have been widely investigated experimentally and computationally for porous materials with nanometer-sized pores.[12–14] For example, the diffusion of 45 nm nanoparticles in polyethylene glycol (PEG)-passivated 300 nm cylindrical pores decreased by a factor of 2 due to hydrodynamic friction.[15] The large diffusion gradients imposed by nanoscale pores can result in (1) cell necrosis and hypoxia if insufficient nutrients and oxygen are delivered to the encased islets, and (2) compromised insulin secretion kinetics due to delayed glucose diffusion.[5,16] The reduced nutrients and oxygen availability due to the slow diffusion can directly impact islet viability in as little as 6 h and cause ~50% decrease in glucose-stimulated insulin secretion.[17] In the clinical setting, the delayed glucose-sensing increases the risks of T1D patients of microvascular complications and cardiovascular diseases.[5] Particularly, chronic hyperglycemia leads to serious microvascular complications,[18] whereas hypoglycemia can

result in cognitive impairment, unconsciousness, seizures, and even death.[18] About 30–40% patients with T1D have impaired awareness of hypoglycemia and this confers a 3 to 6-fold increased risk of severe hypoglycemic events.[19,20]

The slow concentration-dependent diffusion through size-restricted nanoporous membranes can potentially be circumvented by using convection-dominated transport because this would create faster solvent movement under a transmembrane pressure gradient, which in turn would efficiently drag small molecules such as glucose and insulin across membranes to the encapsulated cells. We previously reported that silicon nanopore membrane (SNM) with 7 nm wide slit-shaped pores, used under convective transport, allowed undisturbed passage of glucose and insulin through the membrane, and also reduced the passage of pro-inflammatory cytokines, namely TNF-α, IFN-γ, and IL-1β, by 80%.[10] Therefore, it is important to further investigate the glucose–insulin kinetics of the encapsulated islets under diffusive and convective transport on a physiologically relevant time-scale. In the present study, SNM and silicon micropore membrane (SμM) with 7 and 1000 nm-wide slit-shaped pores respectively, were used to encapsulate mouse islets under diffusive and convective conditions with and without cytokine exposure (Figure 1). The islets were then exposed to varying concentration of glucose inside the reservoir culture medium, and glucose-stimulated insulin responses and islet viability were evaluated. In addition, to determine the immunoprotective effect of the membranes, a highly concentrated cocktail of pro-inflammatory cytokines was added to the circulating system to challenge the encapsulated islets.

2. RESULTS AND DISCUSSION

In this study, we constructed a benchtop flow loop circuit consisting of a single membrane that separated islets from the circulating fluid (Figure 1). Using this system, we characterized the kinetics of glucose-stimulated insulin secretion of SNM- and SμM-encapsulated islets under both convective and diffusive transport modalities. Both types of membranes were fabricated using similar methods,[10] resulting in a pore size of 7 and 1000 nm for SNM and SμM, respectively. We further analyzed the effect of cytokine exposure to the function of SNM- and SμM-encapsulated islets by adding a highly concentrated cocktail of pro-inflammatory cytokines including TNF-α, IL-1β, and IFN-γ to the circuit. The ability of membrane-encapsulated islets to secrete insulin upon changes in glucose concentration was characterized by (see Methods section): (1) computing the stimulation index (SI) and shutdown index (SDI), which reflect the magnitude of stimulatory and shut-down insulin response as a function of changes in glucose concentration, respectively; and (2) characterizing the rate of change in insulin secretion as the ambient fluid changed from low-to-high and high-to-low glucose concentrations. We also assessed the viability of encapsulated-islets in the mockloop circuit at the end of the various experimental conditions.

2.1. Kinetics of Glucose-Stimulated Insulin Secretion of Encapsulated Islets

2.1.1. No Cytokine Exposure—Convection-dominated transport can be used to improve solvent transport by efficiently dragging small molecules across size-restricted pores to encapsulated cells based on transmembrane pressure gradient, thus preventing the delays

associated with concentration-dependent diffusion in nanoporous membranes.[21] On the basis of this principle, we used a benchtop flow loop circuit incorporating membrane-encapsulated islets under applied physiological transmembrane pressure (Figure 1).[22] We observed how encapsulated islets responded to changes in glucose concentration across a single silicon membrane under convective transport (~2 psi transmembrane pressure) or diffusive transport (0 psi transmembrane pressure) using this flow circuit. Unencapsulated islets cultured under static conditions were used as controls. Islets under all conditions reacted quickly to the high glucose concentration (16.6 mM) within the first 10 min by producing more insulin (40 min time point; Figure 2,a). The unencapsulated islets under static culture and SNM-encapsulated islets under diffusion reached the peak of the response 20 min after high glucose exposure, whereas insulin secretion of the SNM-encapsulated islets under convection continued to increase during the entire 30 min duration of high glucose challenge (Figure 2,a). The quick insulin response within 5–10 min of high glucose exposure was consistent with normal functioning islets releasing insulin in a biphasic manner[23,24] (e.g., the first insulin phase appeared within 5–10 min followed by a second sustained phase). However, the second insulin releasing phase was not displayed within this 30 min high glucose exposure window. We suspected that it was due to (1) the insufficient time given to the high glucose challenge; and (2) the 10 min sampling interval, which limited the resolution of the glucoseinsulin kinetics graph. It was previously observed that perifusion with 1 mL/min rate could exhibit the biphasic insulin secretion of mouse islets.[25] Our study with an ultrafiltrate rate (e.g., ~3.5 ul/min) constrained by the intrinsic properties of the membrane and pressure difference required a longer sampling period to ensure sufficient volume collection for insulin detection. This could potentially limit the resolution of the glucose-stimulated insulin secretion curve. The stimulation index (SI), calculated as the ratio of the first insulin collection in the high glucose phase to the last insulin collection in the previous low glucose phase (Immediate Stimulation), were generally comparable among naked islets under static conditions and the SNM-encapsulated islets under convection and diffusion cases, which were 3.92 ± 1.07, 6.38 ± 0.44, and 5.62 ± 1.51, respectively (Figure 2b). However, when the highest level of insulin secretion from high glucose phase was used to calculate the magnitude of stimulation (Maximum Stimulation), the naked islets under static conditions and SNM-encapsulated islets under convection and diffusion cases showed SI of 5.29 ± 0.69, 8.92 ± 1.35, 5.97 ± 1.16, respectively (Figure 2b). The SI of SNM-encapsulated islets under convection showed a 1.49-fold increase than that under diffusion.

Once the circuit was switched back to low glucose concentration (1.6 mM) from 60 to 90 min, the SNM-encapsulated islets under convection exhibited a rapid shutdown in insulin production whereas a gradual decrease in insulin production occurred for the capsule under the diffusive mode. The shut-down index (SDI), calculated as the ratio of the first insulin collection in the subsequent low glucose phase to the last insulin collection in the previous high glucose phase (Immediate Shutdown), showed that the amount of insulin that was secreted significantly decreased for SNM-encapsulated islets under convection (0.20 ± 0.03) compared with the naked islets under static culture (0.59 ± 0.17) and SNM-encapsulated islets under diffusion (0.93 ± 0.19) (Figure 2c). When the lowest level of insulin secretion from the subsequent glucose phase was used to calculate the magnitude of shut down (Maximum Shutdown), the SDI showed that the amount of secreted insulin significantly

decreased for SNM-encapsulated islets under convection (0.11 ± 0.02) compared with the naked islets under static culture (0.40 ± 0.09) and SNM-encapsulated islets under diffusion (0.42 ± 0.11) (Figure 2c). The SDI of SNM-encapsulated islets under convection showed a 3.86-fold decrease compared to that under diffusion. The slow insulin activation and delayed shut-down response associated with diffusive transport is consistent with previous studies on islets encapsulating in hydrogels[26,27] and restricted pore size in the sub-10 nm range.[28] For example, the islet-encapsulating Nanogland device with lateral positioned 3.6 and 5.7 nm nanochannels reported a significant reduction in glucose diffusivity by 40 and 25% compared to the diffusivity in bulk medium, respectively.[28] This delay of insulin shut-down that occurred in the diffusive scenario could potentially lead to problems in the clinical setting, because insulin production would be high in the face of falling blood glucose levels.[18] In contrast, the SNM-encapsulated islets under convection showed the ability to quickly activate and cease insulin production, which is extremely important to simulating the physiological glucose—insulin response.

As illustrated in Table 1, the rate of change in insulin production without cytokine exposure was monitored when conditions transitioned from low-high to high-low glucose phases. The rates of change in insulin activation and cessation were on the same scale in the naked islets under static culture as in the SNM-encapsulated islets under diffusion (0.86 and 0.84 for the stimulation and −0.71 and −0.42 for deactivation, respectively; Table 1). The SNM-encapsulated islets under convection showed 1.16- and 1.19-fold increase in the rate of glucose-stimulated insulin response and 3.82- and 6.45-fold decrease in the rate of insulin shut-down compared with the naked islets under static culture and SNM-encapsulated islets under diffusion, respectively. In short, the magnitude of glucose-stimulated insulin secretion was higher for SNM-encapsulated islets under convection compared to the naked islets under static culture and SNM-encapsulated islets under diffusion as indicated by the SI (Figure 2,b). The SNM-encapsulated islets under convection showed the fastest rate of insulin production (~1 normalized insulin content min^{-1} ($\times 10^{-2}$)) and cessation (approximately −2.7 normalized insulin content min^{-1} ($\times 10^{-2}$)) compared to the other two conditions (Table 1). These data demonstrated that the responsiveness of convection-based SNM encapsulation was significantly better compared to the islet culture under static conditions and SNM encapsulation under diffusion.

Further comparison with the silicon micropore membrane (SμM)-encapsulated islets under convection showed that pressure-driven convection yields faster mass transport as the pore size becomes larger (1 μm). The naked islets under static culture, SNM-encapsulated islets under convection, and SμM-encapsulated islets under convection all quickly released more insulin during high glucose exposure from 40 to 60 min (Figure 2a). Whereas the level of insulin plateaued in the naked islets, the amount of secreted insulin increased in the SNM-encapsulated islets under convection from 50 to 60 min. However, the SμM-encapsulated islets under convection showed a maximum level of secreted insulin at 50 min followed by an immediate concentration drop at 60 min. The difference in the glucose—insulin kinetics between SNM- and SμM-encapsulation under convection during high glucose challenge can be explained by (1) the variation in the ultrafiltration rate produced by two different types of membranes despite efforts to adjust both membranes to obtain the same amount of ultrafiltrate (section 4.3); and (2) possible protein adsorption on the SNM[29,30] that resulted

in the lack of negative feedback inhibition of insulin secretion[31] due to additional fouling resistance (Figure 2a). Furthermore, the SI indicating the magnitude of insulin secretion during prestimulation and stimulation (Immediate Stimulation) were higher for SNM- and SμM-encapsulation under convection compared to naked islets under static conditions, which were 6.38 ± 0.44, 6.44 ± 1.41, and 3.92 ± 1.07, respectively (Figure 2,b). When the highest amount of insulin secretion in the high glucose phase was used to calculate SI (Maximum Stimulation), SμM-encapsulation under convection (8.92 ± 1.34) and SμM-encapsulation under convection (11.8 ± 1.64) showed significantly higher SI compared to naked islets under static conditions (5.29 ± 0.69) (Figure 2b). The SDI calculated from the ratio of insulin secretion from poststimulation and stimulation (Immediate Shutdown) for SNM- and SμM-encapsulation under convection were 0.20 ± 0.03 and 0.25 ± 0.09, which showed a significant decrease in the magnitude of insulin secreted during low glucose exposure compared to the naked islets (0.59 ± 0.17) (Figure 2,c). This trend was also observed for SNM-encapsulation under convection (0.11 ± 0.02), SμM-encapsulation under convection (0.11 ± 0.01), and the naked islets (0.40 ± 0.09) when the SDI was calculated based on the ratio of lowest insulin secretion from poststimulation and stimulation (Maximum Shutdown) (Figure 2c).

In addition, the SμM-encapsulated islets under convection showed the fastest rate of response when switching from low to high glucose condition (3.15 normalized insulin content min^{-1} ($\times 10^{-2}$)) to the high to low glucose situation (−3.36 normalized insulin content min^{-1}($\times 10^{-2}$) (Table 1). The SμM-encapsulated islets under convection demonstrated 3.66- and 3.15-fold increase in the rate of glucose-stimulated insulin response, and 4.73- and 1.24-fold decrease in rate of insulin shut-down compared with the naked islets under static culture and SNM-encapsulated islets under convection, respectively (Table 1). All rates of change in insulin production and cessation were comparable among the naked islets under static culture, SNM-encapsulated islets under diffusion, and SμM-encapsulated islets under diffusion (Table 1). Noticeably, membrane-encapsulation under diffusive scenarios showed a slower insulin response when stimulated with high concentration of glucose (Figure S1). This could be due to the potential boundary layer formation by adsorption of molecules in the nanoscale pores.[29,30] Depending on the choice of membranes and methods to stimulate the islets (diffusion vs convection), all experimental conditions had a SI ranging from 2.89 to 6.44 (Figure S1), which is consistent with typical values (2–20) for healthy mouse islets.[32] Convective conditions with SNM- and SyμM-encapsulation outperformed the pure diffusive scenarios during the glucose–insulin activation and shut-down phases. In particular, convective transport with SμM encapsulation demonstrated superior response in insulin activation, whereas the insulin shut-down was observed to be similar for both SNM and SμM encapsulation under convection.

2.1.2. Cytokine Exposure—A highly concentrated solution of pro-inflammatory cytokines consisting of TNF-α, IFN-γ, and IL-1β was used to investigate how the glucose–insulin kinetics of SNM-encapsulated islets are influenced by cytokine exposure. When challenged with high glucose concentration, SNM-encapsulated islets under convection immediately secreted insulin to the maximum level within first 10 min followed by a slight decrease in insulin secretion in the next 20 min (Figure 3,a). However, SNM-encapsulated

islets under diffusion showed an incremental increase in insulin secretion during high glucose exposure. Although we also observed an increase in the insulin secretion level for the naked islets under static culture during the high glucose challenge, the maximum level of insulin secreted was not as amplified as the other two conditions. Furthermore, the magnitude of insulin secretion during prestimulation and stimulation (Immediate Stimulation) was significantly different among the naked islets under static conditions, and SNM encapsulation under convection and diffusion as indicated by the SI, which were 2.98 ± 0.06, 6.22 ± 0.69, and 4.29 ± 0.34, respectively (Figure 3,b). When the highest amount of insulin secretion in the high glucose phase was used to calculate SI (Maximum Stimulation), SNM-encapsulation under convection (6.50 ± 0.42) showed an increase in SI compared to SNM-encapsulation under convection (4.99 ± 0.51) and naked islets under static conditions (3.85 ± 1.51) (Figure 3b). As the circuit was switched back to low glucose concentration, SNM-encapsulated islets under convection showed the most significant drop in insulin secretion compared to the naked islets and SNM encapsulation under diffusion (Figure 3,a). The SDI calculated based on the ratio of insulin secretion from poststimulation and stimulation (Immediate Shutdown) for naked islets, and SNM encapsulation under convection and diffusion were 1.1 ± 0.36, 0.42 ± 0.19, and 0.8 ± 0.12, respectively (Figure 3c). The similar trend was observed for SNM-encapsulation under convection (0.26 ± 0.02), SNM-encapsulation under diffusion (0.57 ± 0.15), and the naked islets (0.70 ± 0.12) when the SDI was calculated based on the ratio of lowest insulin secretion from poststimulation and stimulation (Maximum Shutdown) (Figure 3c). Further analysis of the rate of change in insulin production from low to high glucose stimulation showed that SNM-encapsulated islets under convection produced 2.89 normalized insulin content min^{-1} ($\times 10^{-2}$), whereas naked islets under static conditions and SNM-encapsulated islets under diffusion produced 0.22 and 0.73 normalized insulin content min^{-1} ($\times 10^{-2}$) (Table 2). The rate of change in insulin production from high to low glucose cessation of SNM-encapsulated islets under convection was −1.76 normalized insulin content min^{-1} ($\times 10^{-2}$), whereas that of the naked islets under static culture and SNM-encapsulated islets under diffusion were −0.092 and −0.32 normalized insulin content min^{-1} ($\times 10^{-2}$). The SNM-encapsulated islets under convection exhibited a 13.1- and 3.96-fold increase in the rate of insulin production compared with naked islets and SNM encapsulation under diffusion respectively, when conditions were changed from low to high glucose exposure with cytokines. The SNM-encapsulated islets under convection also demonstrated a 19.1- and 5.5-fold increase in the rate of shutting down insulin secretion from high to low glucose conditions compared with naked islets and SNM encapsulation under diffusion. In summary, the SNM-encapsulated islets under convection exceeded both naked islets and SNM encapsulation under diffusion in terms of the magnitude of insulin produced when stimulated with high level of glucose (Figure 3b, c) and the rate at which insulin was produced and ceased due to changes in glucose concentration (Table 2).

Unlike the SNM-encapsulated islets under convection in which the maximum level of insulin secreted within 10 min of high glucose challenge, SμM-encapsulation under convection showed a continuous rise in insulin secretion and reached the highest peak within 30 min of high glucose exposure (Figure 3a). Moreover, SNM-encapsulated islets under convection exhibited the largest magnitude of glucose-stimulated insulin secretion

possessing a SI value of 6.22 ± 0.69, which was significantly higher than that for the SμM-encapsulation case with a SI value of 4.66 ± 0.07 (Immediate Stimulation) (Figure 3b). When the highest amount of insulin secretion in the high glucose phase was used to calculate SI (Maximum Stimulation), SNM- and SμM-encapsulation under convection (6.50 ± 0.42 and 6.37 ± 0.11) showed an increase in SI compared to naked islets under static conditions (3.85 ± 1.51) (Figure 3b). However, the SDI for immediate shutdown of SNM- and SμM-encapsulated islets under convection were similar in which the SDI were 0.42 ± 0.19 and 0.40 ± 0.04, respectively (Figure 3c). The same trend was observed when examining the SDI of SNM- and SμM-encapsulation under convection (0.26 ± 0.02 and 0.28 ± 0.04) and the naked islets (0.70 ± 0.12) where the SDI was calculated based on the ratio of lowest insulin secretion from poststimulation and stimulation (Maximum Shutdown) (Figure 3c). Although the absolute amount of insulin released was higher in SμM-encapsulation under convection (Figure 3a), the SI and SDI of SNM- and SμM-encapsulation under convection were similar (Figure 3b, c). The relative large pore size of SμM could easily allow the entry of cytokines but probably due to the membrane hindrance and protein adsorption, not all cytokines were infiltrated to induce cell death. Further analysis of the rate of changes in insulin production was calculated for SμM-encapsulated islets under convection, which showed a 1.46-fold decrease and 1.61-fold increase compared with SNM-encapsulated islets under convection in transitioning from low to high glucose stimulation and from high to low glucose shut-down, respectively (Table 2). Noticeably, all diffusive conditions with both SNM- and SμM-encapsulation showed reduction in the magnitude of insulin produced as well as decline in the rate of insulin production compared to all convective scenarios (Figure S2 and Table S1). In summary, convective transport with SNM encapsulation demonstrated better performance than SμM-encapsulation in terms of the magnitude of insulin produced and ceased during high and low glucose phases as indicated by SI and SDI factors under cytokine exposure (Figure 3), whereas the rate of changes in insulin secretion was similar between the two (Table 2).

Comparing previous conditions (section 2.1.1) that were not subjected to cytokines, we observed that conditions with cytokine exposure had a slight decrease in SI values (Figure S2). We observed no significant difference in the magnitude of insulin secreted before and after cytokine exposure for SNM-encapsulation under convection (SI) (Immediate Stimulation): 6.38 ± 0.44 and 6.23 ± 0.69, respectively) (Figures 2b and 3b), whereas the SμM-encapsulation under convection and naked islets under static culture all declined slightly in their SI values (Immediate Stimulation): SμM-encapsulation under convection dropped from 6.44 ± 1.41 to 4.66 ± 0.07 (Figures 2b and 3b), and naked islets decreased from 3.92 ± 1.06 to 2.98 ± 0.06 (Figures 2b and 3b). The naked islets under static culture showed a higher SDI value (Immediate Shutdown) with cytokine exposure (0.59 ± 0.17) (Figure 2c) than the no-cytokine condition (1.1 ± 0.36) (Figure 3c), whereas SNM-and SμM-encapsulation under convection showed consistent SDI values (Immediate Shutdown) before and after cytokines were added (Figures 2c and 3c). When switching from high to low glucose conditions, the naked islets showed a large variation in the SDI value (Immediate Shutdown), indicating partial loss of islet regulatory function with insulin (Figure 3a, c). In contrast, both membrane-encapsulated conditions showed sharp drop in insulin production once they were switched back to low glucose environment (Figure 3). Cytokines including

TNF-α, IFN-γ, and IL-1β are known to be synergistically cytotoxic through a cascade of inflammatory events such as production of nitric oxide and chemokines, and trigger of endoplasmic reticulum stress to cause loss of islet viability and functionality.[33,34] We speculated that cytokines damaged the naked islets as shown by their changes in SI and SDI values mentioned above, whereas the selectivity of the SNM and SμM membranes hindered cytokine infiltration and preserved islet function.

2.2. Islet Viability

In addition to the glucose–insulin kinetics of SNM- and SμM-encapsulation described above, we investigated the islet viability to understand if cytokines caused excessive islet dysfunction (Figure 4). The naked islets with cytokine exposure showed significantly more cell death compared to all other groups including SNM- and SμM-encapsulation under convection (Figure 4a). All membrane-associated diffusive conditions showed normal health comparable to the untreated naked islets under static culture (Figure S3). Some level of cytokine-induced death damage was observed in the SμM-encapsulation under convection as a result of their inability to completely exclude cytokines likely due to the large membrane pore size (Figure 4b). However, the islet death in the SμM-encapsulation under convection was not as significant as in the control scenario with naked islets. The SNM-encapsulated islets under convection with cytokine exposure showed similar viability compared to SNM-encapsulating and healthy control conditions without cytokines. These observations confirm that membrane protection afforded by SNM provides sufficient immunoisolation to support viability (section 2.2) and functional performance of the encapsulated islets, which is indicated by the glucose-kinetics data (section 2.1).

3. CONCLUSIONS

In this study, we characterized the glucose–insulin kinetics of an improved silicon nanopore membrane, SNM, for the encapsulation of pancreatic islets under convective flow. The glucose–insulin responsiveness of membrane-encapsulated islets was analyzed under a series of low, high, and low glucose challenge by (1) SI and SDI values, which show the magnitude of insulin secreted when transitioning from low to high glucose condition or vice versa; and (2) rate of change in insulin secretion, which indicates how quickly the system responds from low to high glucose condition or vice versa. On the basis of these parameters, we found that convective mode performed better than diffusive mode in both SNM and SμM encapsulations. In addition, once exposed with cytokines, convective transport with SNM encapsulation demonstrated superior performance over SμM encapsulation in terms of the magnitude of insulin produced and ceased during high and low glucose phases with healthy islet viability, whereas the rate of changes in insulin secretion was on the same scale as that for the SμM encapsulation. In summary, SNM encapsulation under convective transport enables rapid glucose–insulin sensing to activate and cease insulin production based on the surrounding glucose concentration while retaining healthy islet viability even under cytokine exposure. Our data demonstrate the importance of using convective transport to obtain a faster insulin activation and shut-down, which is a critical issue to address in many islet-encapsulating devices[5,35] with undesired delay in glucose–insulin response. Successful islet encapsulation with selective SNM under convective transport could potentially lower the

immunosuppressive drugs and their side effects resulted from current therapies, lead to the possibility of using xenogeneic or stem-cell derived cell sources to overcome donor shortage, and reduce dangerous episodes of hypoglycemia for T1D patients in the future.

4. MATERIALS AND METHODS

4.1. Experimental Overview

SNM were designed to have an active membrane area (6 × 6 mm) consisting of ~1 × 10^6 rectangular slit pores with an average pore size of 7 nm in width, 2 μm in length, and 300 nm in depth.[10] The surface of SNM was coated with polyethylene glycol (PEG) to minimize protein fouling. All SNM used in this study exhibited a measured average pore size of ~7 nm postpegylation. The control silicon micropore membrane (SμM) had the same design, but with an average pore size of 1000 nm. In this study, we observed how encapsulated islets responded to changes in glucose concentration across a single silicon membrane under convective transport (~2 psi transmembrane pressure) or diffusive transport (0 psi transmembrane pressure) using a pressure-driven filtration circuit. Convective studies were performed at a trans-membrane pressure of 2 psi which is consistent with typical physiological pressure difference between the artery and vein.[10,22] We further tested the glucose–insulin response by using highly concentrated cytokine solution in the circuit. We subsequently analyzed the respective stimulation index (SI) and shut-down index (SDI) of encapsulated islets under convective and diffusive conditions. We also studied the rate of change in insulin production based on the slopes of curves that were fitted on glucose–insulin kinetics graphs to describe the quickness of insulin being secreted as glucose concentration changes. Finally, we characterized the viability of encapsulated islets in the pressure-driven filtration assembly under various mass transfer and cytokine exposure conditions.

4.2. Substrate Preparation

4.2.1. Silicon Nanopore Membranes (SNM) and Silicon Micropore Membrane (SμM): Architecture and Fabrication—Silicon nanopore membranes (SNM) have been prototyped from silicon substrates by MEMS technology as previously reported[30,36,37] with some modifications.[10] Briefly, the process used the growth of a thin SiO_2 (oxide) layer on 400 μm-thick double side polished (DSP) silicon wafers followed by a low pressure chemical vapor deposition (LPCVD) of polysilicon (~500 nm). The wafers were then specifically patterned, dry oxidized, wet etched, deposited with a second polysilicon layer, and finally blanket-etched until 400 nm of polysilicon remained and the underlying vertical oxide layer was exposed. The vertical sacrificial oxide layer defined the critical nanoscale pore size of the membranes. The low temperature oxide (LTO) (~1 μm) was deposited onto polysilicon of the wafers to serve as the hard mask for membrane protection. Deep reactive ion etching (DRIE) removed the backside of each window until membranes were disclosed. Eventually, the sacrificial oxide was etched away in 49% hydrofluoric acid (HF) during the final step of the fabrication process to leave behind open nanoscale slit pores. The wafers were subsequently cut into 1 × 1 cm chips with an effective area of 6 × 6 mm^2 containing 1500 windows each, with a total of 10^6 pores per membrane. Each rectangular pore was 7 nm in width, 300 nm in depth, and 2 μm in length. Silicon micropore membrane (SμM) were

fabricated to produce wafer-scale arrays of 500 nm by 4 μm rectangular slit pores with 1000 nm-wide slit width using similar process. The wafers were diced to form 1 × 1 cm chips with an effective area of 6 × 6 mm^2 containing 1500 windows each, with a total of 3.12^6 pores per membrane. All membranes were cleaned using a conventional "piranha" clean procedure, which involved a 20 min-immersion in 3:1 sulfuric acid (H_2SO_4)/hydrogen peroxide (H_2O_2) mixture, followed by thorough rinses in deionized (DI) water.

4.2.2. Surface Modification of SNM with poly(ethylene glycol) (PEG)—SNM were covalently modified with PEG using a previously reported protocol[38] with some modifications to prevent protein fouling on the membrane surface. The technique used for PEG attachment involved a single reaction step which covalently couples silicon surface silanol group (Si–OH) to a chain of PEG polymer through a trimethoxysilane group forming a Si–O–Si–PEG sequence. Briefly, SNM were immersed in a solution of 3 mM 2-[methoxy-(polyethyleneoxy)propyl]trimethoxysilane (PEG-silane) (Gelest: SIM6492.7) in toluene for 2 h at 70 °C. A series of extensive washing steps involving toluene, ethanol, and DI water were used to rinse away unbounded PEG residue.

4.2.3. Hydraulic Permeability for SNM Pore Size Characterization—An automated mass and pressure measurement system was utilized for characterizing liquid flow through the SNM under a tangential-flow filtration operation.[10] The pore size of the SNM can be related to filtration flow parameters using

$$h = \sqrt[3]{\frac{12\mu l Q}{n w \Delta P}} \quad (1)$$

where h is pore width, μ is the viscosity, l is the membrane thickness, Q is the volumetric flow rate, n is the number of pores per membrane, w is the pore length, and ΔP is the transmembrane pressure. To assemble the overall system for SNM pore size characterization (Figure S4), we applied airthrough a syringe pump (Sigma: Z675709) into a water reservoir. Water was circulated by a peristaltic pump (Masterflex: 07551–00) through a differential pressure transducer (Omega: PX429 015GI), a flow cell with enclosed membrane, and returned to the original water reservoir. The flow cell was assembled with the SNM submerged under water to remove air bubbles from all compartments. Specifically, a membrane was positioned with the polysilicon interface facing down with a customized silicone gasket positioned on top of the membrane, followed by the final placement of a filtrate chamber on top of the gasket. All sections were fastened together and secured to the base with hand-tightened hex bolts until the gasket was visibly compressed. The ultrafiltrate permeated through the membrane was routed to a liquid collection container that rested on a precision mass balance (Mettler Toledo: XS205). Measurements from the differential pressure transducer and the mass balance were automatically collected with a data acquisition laptop. A typical membrane hydraulic permeability test consisted of 5 mL/min flow rate and 4 pressure cycles (5, 1, 5, and 1 psi) for durations of 150 s each. Using the specifications for pore length, membrane thickness, and total number of pores provided based on individual wafer designs, the average pore size of SNM was calculated using eq 1.

All SNM membranes in this study were surface-modified with PEG and exhibited an average pore size of ~7 nm.

4.3. Culture of Membrane-Encapsulated Islets in the Pressure-Driven Filtration Assembly

All procedures described involving isolation of mouse islets were performed in accordance with protocols approved by the Institutional Animal Care and Use Committee (IACUC) at the University of California, San Francisco (UCSF). Mouse islets were isolated from 8 to 10-week-old male B6 mice (Jackson Laboratories) based on previously described protocols.[10] Harvested islets were maintained in suspension culture with RPMI 1640 with L-glutamine and 11.1 mM glucose (Gibco: 11875–093), 10% fetal bovine serum (FBS) (Gibco: 16000), and 1% penicillin-streptomycin (P/S) (UCSF Cell Culture Facility: CCFGK003) for overnight to 1 day prior to membrane encapsulation and subsequent assessment of glucose-stimulated insulin response.

We assembled a mock-loop circuit with two flow cell components.[10] Briefly, one SNM with customized silicone gasket frames were sandwiched in between two flow cell components. A group of 40–50 mouse islets were introduced into the bottom chamber separated by the SNM from the circulating fluid (5 mL/min) in the top chamber. A peristaltic pump drove the fluid through the top of the flow cell component, and finally back to the original medium reservoir. For convective experiments, a three-way valve was used to create flow resistance for a physiological pressure difference ~2 psi between the top and the bottom compartments of the flow cell. The membrane Peclet number (Pe) for the pressure-driven ultrafiltration system was significantly greater than 1, suggesting that convective transport dominates. For diffusive experiments, no transmembrane pressure was induced and fluid still circulated throughout the system. To study the effects of cytokines on SNM-encapsulated islets, solution consisting of mouse cytokines TNF-α (2000 U/mL), IFN-γ (1000 U/mL), and IL-1β (10 000 U/mL) was added to the original reservoir. Silicon membranes with 1 μm-wide slit pores (SμM) were used as the control with adjusted pressure (~0.127 psi) and flow rate (~20 μL/min) to produce similar amount of ultrafiltrate as the SNM in this mock-loop system. Naked mouse islets cultured under static conditions in the Petri dish were also used as controls.

4.3.1. Glucose Challenge in the Pressure-Driven Filtration Mock-Loop System

—The membrane-encapsulated mouse islets in the mock-loop systems were exposed to a series of low (1.6 mM), high (16.6 mM), and low (1.6 mM) glucose (Gibco 11879) stimulation for 30 min each. Supernatant was sampled every 10 min from the bottom islet chamber during this series of glucose challenge. For convective experiments, an ultrafiltrate rate of ~3.5 ul/min was observed for the SNM with ~7 nm pore size and the same ultrafiltrate rate was obtained for the SμM with lowered transmembrane membrane pressure and system flow rate. For diffusive experiments, islet chambers were refilled after individual sampling to ensure that the volume of islet chamber was kept constant at all time. This step minimized any bubbles that might potentially be formed during the process which could hinder mass transfer within the system. Insulin content was measured with mouse insulin enzyme-linked immunosorbent assay (ELISA) kits (Mercodia 10–1247–01) with accounted dilutions and normalized by extracted total protein concentration (Thermo 78505; 23225).[39]

Naked mouse islets were also challenged under static culture condition as controls. About 7–10 μL chamber fluid per islet were used in all cases.

4.3.2. Analysis of Stimulation Index (SI) and Shut-down Index (SDI)—A stimulation index was calculated as the ratio of stimulated to basal insulin secretion. In our study, the stimulation index (SI) was the ratio of (1) the first insulin collection point in the high glucose phase to the last insulin collection point of the previous low glucose phase (Immediate Stimulation), and (2) the highest insulin secretion in the high glucose phase to the last insulin collection point of the previous low glucose phase (Maximum Stimulation). The shut-down index (SDI) was calculated as the ratio of (1) the first insulin collection point in the subsequent low glucose phase to the last insulin collection point in the high glucose phase (Immediate Shutdown), and (2) the lowest insulin secretion in the subsequent low glucose phase to the last insulin collection point in the high glucose phase (Maximum Shutdown). The stimulation index indicates the magnitude of insulin released as stimulated by a higher concentration of glucose, whereas the shut-down index reflects the magnitude of cessation in insulin production once glucose concentration returns to normal.

4.3.3. Analysis of Rate of Change in Insulin Secretion—The rate of change in insulin secretion was calculated for the stimulation and shutdown phases. For the stimulation phase, a first-order curve was fitted on the glucose–insulin kinetic graph with the last point of insulin produced during low glucose exposure to the highest point of insulin produced during high glucose exposure. For the shut-down phase, a first-order curve was fitted on the glucose–insulin kinetic graph with the last point of insulin produced during high glucose exposure to the first point of insulin produced during low glucose exposure. The rate of change was obtained by taking derivatives of those curves to study the quickness of insulin being secreted during changes in glucose concentration.

4.3.4. Islet Viability—Islet viability was assessed by utilizing a two-color fluorescence cell viability assay (LIVE/DEAD Cell Imaging Kit; Invitrogen R37601). Briefly, mouse islets were incubated in the assay staining reagents for 15 min at room temperature followed by extensive washes in PBS to remove excess staining. Images of mouse islets were obtained using laser scanning Nikon Spectral C1si confocal microscope (Nikon Instruments). Viability of islets was calculated based on the percentage of live cells in the islets as described by protocol on assessment of islet viability by fluorescent dyes from Department of Surgery Division of Transplantation at University of Wisconsin–Madison.[40]

4.4. Statistical Analysis

Sample pairs were analyzed using Student's *t* test. Multiple samples were evaluated with one-way or two-way analysis of variance (ANOVA) followed by Bonferroni and multiple comparison using Graphpad Prism software (San Diego, CA). A p value of <0.05 was accepted as statistically significant for all analyses.

Supplementary Material

Refer to Web version on PubMed Central for supplementary material.

Acknowledgments

This research was supported by National Science Foundation (NSF) Graduate Research Fellowship (S.S.), Harry Wm. & Diana V. Hind Distinguished Professorship in Pharmaceutical Sciences II (S.R.), the QB3 J&J Bridging-the-Gap Award, the UCSF CTSI Catalyst Award, and the Juvenile Diabetes Research Foundation (JDRF). We thank colleagues Vinh Nguyen and Vi Dang for their help in mouse islet isolation.

References

1. Shapiro AM, Lakey JR, Ryan EA, Korbutt GS, Toth E, Warnock GL, Kneteman NM, Rajotte RV. Islet transplantation in seven patients with type 1 diabetes mellitus using a glucocorticoid-free immunosuppressive regimen. N Engl J Med. 2000; 343(4):230–8. [PubMed: 10911004]
2. Gruessner AC, Sutherland DE, Gruessner RW. Pancreas transplantation in the United States: a review. Curr Opin Organ Transplant. 2010; 15(1):93–101. [PubMed: 20009932]
3. Hirshberg B, Rother KI, Digon BJ 3rd, Lee J, Gaglia JL, Hines K, Read EJ, Chang R, Wood BJ, Harlan DM. Benefits and risks of solitary islet transplantation for type 1 diabetes using steroid-sparing immunosuppression: the National Institutes of Health experience. Diabetes Care. 2003; 26(12):3288–95. [PubMed: 14633816]
4. Markmann JF, Deng S, Huang X, Desai NM, Velidedeoglu EH, Lui C, Frank A, Markmann E, Palanjian M, Brayman K, Wolf B, Bell E, Vitamaniuk M, Doliba N, Matschinsky F, Barker CF, Naji A. Insulin independence following isolated islet transplantation and single islet infusions. Ann Surg. 2003; 237(6):741–9. [PubMed: 12796569]
5. Song S, Roy S. Progress and challenges in macroencapsulation approaches for type 1 diabetes (T1D) treatment: Cells, biomaterials, and devices. Biotechnol Bioeng. 2016; 113(7):1381–402. [PubMed: 26615050]
6. Chang TM. Semipermeable Microcapsules. Science. 1964; 146(3643):524–5. [PubMed: 14190240]
7. Colton CK. Implantable Biohybrid Artificial Organs. Cell Transplantation. 1995; 4(4):415–436. [PubMed: 7582573]
8. Iwata H, Morikawa N, Fujii T, Takagi T, Samejima T, Ikada Y. Does immunoisolation need to prevent the passage of antibodies and complements? Transpl Proc. 1995; 27(6):3224–3226.
9. Cardozo AK, Proost P, Gysemans C, Chen MC, Mathieu C, Eizirik DL. IL-1 beta and IFN-gamma induce the expression of diverse chemokines and IL-15 in human and rat pancreatic islet cells, and in islets from pre-diabetic NOD mice. Diabetologia. 2003; 46(2):255–266. [PubMed: 12627325]
10. Song S, Faleo G, Yeung R, Kant R, Posselt AM, Desai TA, Tang Q, Roy S. Silicon nanopore membrane (SNM) for islet encapsulation and immunoisolation under convective transport. Sci Rep. 2016; 6:23679. [PubMed: 27009429]
11. Deen WM. Hindered Transport of Large Molecules in Liquid-Filled Pores. AIChE J. 1987; 33(9): 1409–1425.
12. Han R, Wang GF, Qi SD, Ma CB, Yeung ES. Electrophoretic Migration and Axial Diffusion of Individual Nano-particles in Cylindrical Nanopores. J Phys Chem C. 2012; 116(34):18460–18468.
13. Jiang XQ, Mishra N, Turner JN, Spencer MG. Diffusivity of sub-1,000 Da molecules in 40 nm silicon-based alumina pores. Microfluid Nanofluid. 2008; 5(5):695–701.
14. Nagumo R, Takaba H, Nakao SI. Accelerated computation of extremely 'slow' molecular diffusivity in nanopores. Chem Phys Lett. 2008; 458(4–6):281–284.
15. Chen F, Neupane B, Li P, Su W, Wang G. Investigating axial diffusion in cylindrical pores using confocal single-particle fluorescence correlation spectroscopy. Electrophoresis. 2016; 37(15–16): 2129–38. [PubMed: 27196052]
16. Tomei AA, Manzoli V, Fraker CA, Giraldo J, Velluto D, Najjar M, Pileggi A, Molano D, Ricordi C, Stabler CL, Hubbell JA. Device design and materials optimization of conformal coating for islets of Langerhans. Proc Natl Acad Sci USA. 2014; 111(29):10514–10519. [PubMed: 24982192]
17. Dionne KE, Colton CK, Yarmush ML. Effect of hypoxia on insulin secretion by isolated rat and canine islets of Langerhans. Diabetes. 1993; 42(1):12–21. [PubMed: 8420809]
18. Cryer PE. Minireview: Glucagon in the Pathogenesis of Hypoglycemia and Hyperglycemia in Diabetes. Endocrinology. 2012; 153(3):1039–1048. [PubMed: 22166985]

19. Geddes J, Schopman JE, Zammitt NN, Frier BM. Prevalence of impaired awareness of hypoglycaemia in adults with Type 1 diabetes. Diabetic Med. 2008; 25(4):501–4. [PubMed: 18387080]
20. Hopkins D, Lawrence I, Mansell P, Thompson G, Amiel S, Campbell M, Heller S. Improved biomedical and psychological outcomes 1 year after structured education in flexible insulin therapy for people with type 1 diabetes: the U.K. DAFNE experience. Diabetes Care. 2012; 35(8): 1638–42. [PubMed: 22619082]
21. Maher, JF. Replacement of Renal Function by Dialysis: A Text Book of Dialysis. Springer Science & Business Media; Berlin: 1989. p. 1188
22. Sircar, S. Principles of Medical Physiology. Thieme; Stuttgart, Germany: 2008. p. 793
23. Hedeskov CJ. Mechanism of glucose-induced insulin secretion. Physiol Rev. 1980; 60(2):442–509. [PubMed: 6247727]
24. Rorsman P, Eliasson L, Renstrom E, Gromada J, Barg S, Gopel S. The Cell Physiology of Biphasic Insulin Secretion. News Physiol Sci. 2000; 15:72–77. [PubMed: 11390882]
25. Zawalich WS, Yamazaki H, Zawalich KC. Biphasic insulin secretion from freshly isolated or cultured, perifused rodent islets: comparative studies with rats and mice. Metab Clin Exp. 2008; 57(1):30–39. [PubMed: 18078856]
26. de Vos P, Smedema I, van Goor H, Moes H, van Zanten J, Netters S, de Leij LFM, de Haan A, de Haan BJ. Association between macrophage activation and function of micro-encapsulated rat islets. Diabetologia. 2003; 46(5):666–673. [PubMed: 12750768]
27. Jesser C, Kessler L, Lambert A, Belcourt A, Pinget M. Pancreatic islet macroencapsulation: a new device for the evaluation of artificial membrane. Artif Organs. 1996; 20(9):997–1007. [PubMed: 8864021]
28. Sabek OM, Ferrati S, Fraga DW, Sih J, Zabre EV, Fine DH, Ferrari M, Gaber AO, Grattoni A. Characterization of a nanogland for the autotransplantation of human pancreatic islets. Lab Chip. 2013; 13(18):3675–88. [PubMed: 23884326]
29. Desai TA, Hansford DJ, Leoni L, Essenpreis M, Ferrari M. Nanoporous anti-fouling silicon membranes for biosensor applications. Biosens Bioelectron. 2000; 15(9–10):453–62. [PubMed: 11419640]
30. Fissell WH, Dubnisheva A, Eldridge AN, Fleischman AJ, Zydney AL, Roy S. High-Performance Silicon Nanopore Hemofiltration Membranes. J Membr Sci. 2009; 326(1):58–63.
31. Ammon HP, Reiber C, Verspohl EJ. Indirect evidence for short-loop negative feedback of insulin secretion in the rat. J Endocrinol. 1991; 128(1):27–34. [PubMed: 1999674]
32. Carter JD, Dula SB, Corbin KL, Wu R, Nunemaker CS. A practical guide to rodent islet isolation and assessment. Biol Proced Online. 2009; 11:3–31. [PubMed: 19957062]
33. Cnop M, Welsh N, Jonas JC, Jorns A, Lenzen S, Eizirik DL. Mechanisms of pancreatic beta-cell death in type 1 and type 2 diabetes: many differences, few similarities. Diabetes. 2005; 54(Suppl 2):S97–S107. [PubMed: 16306347]
34. Ammendrup A, Maillard A, Nielsen K, Aabenhus Andersen N, Serup P, Dragsbaek Madsen O, Mandrup-Poulsen T, Bonny C. The c-Jun amino-terminal kinase pathway is preferentially activated by interleukin-1 and controls apoptosis in differentiating pancreatic beta-cells. Diabetes. 2000; 49(9):1468–76. [PubMed: 10969830]
35. Weber LM, Lopez CG, Anseth KS. Effects of PEG hydrogel crosslinking density on protein diffusion and encapsulated islet survival and function. J Biomed Mater Res Part A. 2009; 90(3): 720–729.
36. Fissell WH, Humes HD, Fleischman AJ, Roy S. Initial characterization of a nanoengineered ultrafiltration membrane. J Am Soc Nephrol. 2002; 13:602a.
37. Fissell WH, Manley S, Westover A, Humes HD, Fleischman AJ, Roy S. Differentiated growth of human renal tubule cells on thin-film and nanostructured materials. ASAIO J. 2006; 52(3):221–227. [PubMed: 16760708]
38. Papra A, Gadegaard N, Larsen NB. Characterization of ultrathin poly(ethylene glycol) monolayers on silicon substrates. Langmuir. 2001; 17(5):1457–1460.
39. Alarcon C, Boland BB, Uchizono Y, Moore PC, Peterson B, Rajan S, Rhodes OS, Noske AB, Haataja L, Arvan P, Marsh BJ, Austin J, Rhodes CJ. Pancreatic beta-Cell Adaptive Plasticity in

Obesity Increases Insulin Production but Adversely Affects Secretory function. Diabetes. 2016; 65(2):438–50. [PubMed: 26307586]

40. Hanson MS, Park EE, Sears ML, Greenwood KK, Danobeitia JS, Hullett DA, Fernandez LA. A simplified approach to human islet quality assessment. Transplantation. 2010; 89(10):1178–88. [PubMed: 20182409]

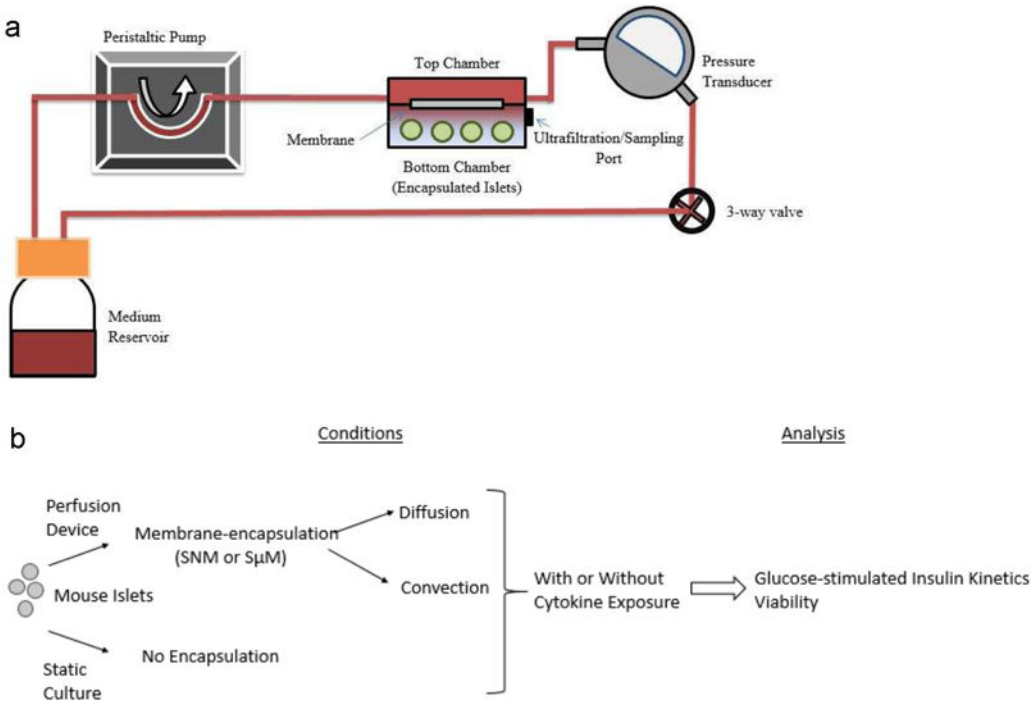

Figure 1.

Diagrams of the experimental conditions. (a) Schematic diagram of the perfusion device for in vitro assessment of glucose-stimulated insulin secretion from membrane-encapsulated mouse islets. A peristaltic pump circulated media through the upper compartment of a two-layered flow cell separated by a membrane (SNM or SμM). Islets were encapsulated in the bottom chamber. A 3-way valve was incorporated into the system to establish transmembrane pressure to create either diffusive or convective condition. A set of 75 perfusate samples was collected from the bottom chamber at 10 min intervals for up to 1.5 h. The bottom chamber was replenished with media following each collection and correction for dilution was made in calculation of the insulin concentration. (b) Schematic of all experimental conditions including the membrane-encapsulated islets under diffusion and convection (device, diffusion vs device, convection), and static culture as control (no device, no perfusion). A mixture of cytokines was also added to examine the effect on each condition (+Ck). The glucose-stimulated insulin kinetics and viability were analyzed for all conditions.

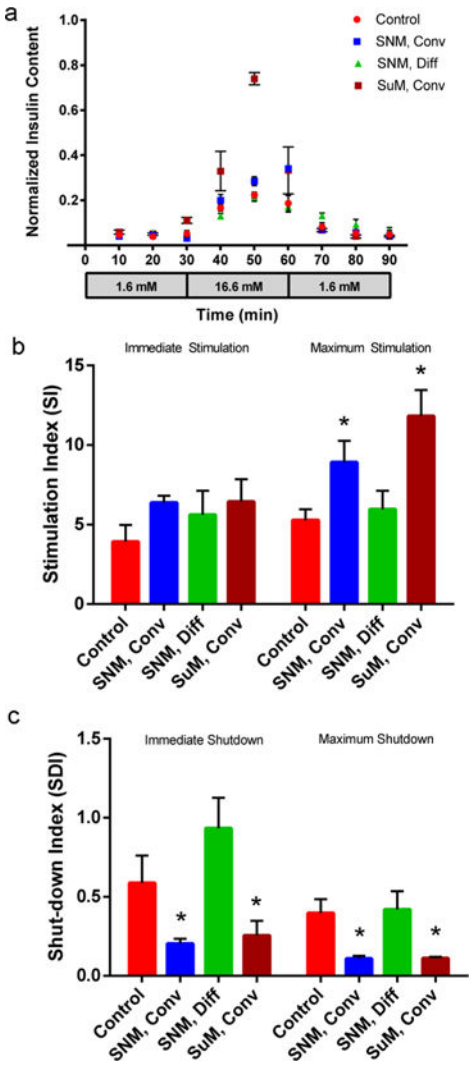

Figure 2.

Glucose—insulin kinetics of membrane-encapsulated islets under convection and diffusion without cytokine exposure. (a) Insulin release kinetics of membrane-encapsulated mouse islets during 90 min low-high- low (1.6, 16.6, and 1.6 mM) glucose stimulation under convective (2 psi) (Conv) and diffusive transport (Diff) without subjection to cytokines. The naked islets cultured under static conditions served as controls (Control). The SNM-and SμM- encapsulated islets under convective transport (SNM, Conv & SμM, Conv) exhibited higher insulin secretion following stimulation at high glucose concentration and faster insulin release kinetics in response compared to those under diffusive transport (Control & SNM, Diff) (,ean ± SEM, $n \geq 3$). (b) Stimulation index (SI) was calculated as the ratio of (1) the first insulin collection in the high glucose phase at 40 min to the last insulin collection point of the previous low glucose phase at 30 min (Immediate Stimulation), and (2) the highest insulin secretion in the high glucose phase to the last insulin collection point of the previous low glucose phase at 30 min (Maximum Stimulation). The SI indicates the magnitude of insulin released as stimulated by a higher concentration of glucose. Without cytokine exposure, SNM- encapsulated islets under convection (SNM, Conv) and diffusion

(SNM, Diff), SμM-encapsulated islets under convective transport (SμM, Conv), and the naked islets cultured under static conditions (Control) all exhibited similar magnitude of glucose-induced insulin secretion when transitioning from low glucose to high glucose (Immediate Stimulation). However, the SI of SNM- and SμM-encapsulated islets under convection (SNM, Conv & SμM, Conv) was the highest compared to that under diffusion (SNM, Diff) and the naked islets cultured under static conditions (Control) when the highest insulin secretion in the high glucose phase was used (Maximum Stimulation) (mean ± SEM, $n \geq 3$). (c) Shut-down index (SDI) was the ratio of (1) the first insulin collection point in the subsequent low glucose phase at 70 min to the last insulin collection point in the high glucose phase at 60 min (Immediate Shutdown), and (2) the lowest insulin secretion in the subsequent low glucose phase to the last insulin collection point in the high glucose phase at 60 min (Maximum Shutdown). The SDI reflects the magnitude of cessation in insulin production once glucose concentration returns to normal. Without cytokine exposure, SNM- and SμM-encapsulated islets under convection (SNM, Conv & SμM, Conv) exhibited the highest magnitude of insulin reduction compared to the diffusive condition (SNM, Diff) and the naked islet culture (Control) as glucose dropped low (Immediate Shutdown & Maximum Shutdown) (mean ± SEM, $n \geq 3$, $^*p < 0.05$).

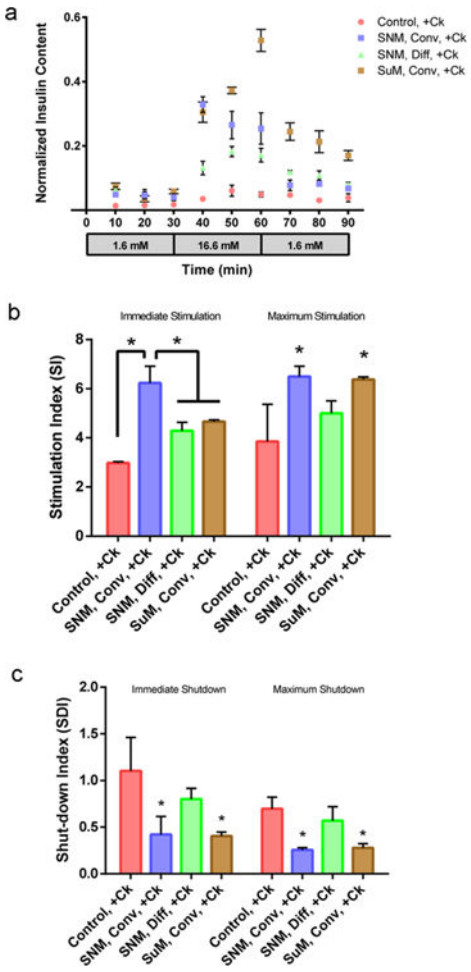

Figure 3.

Glucose—insulin kinetics of membrane-encapsulated islets under convection and diffusion with cytokine exposure. (a) Insulin release kinetics of membrane-encapsulated mouse islets during 90 min low—high—low (1.6, 16.6, and 1.6 mM) glucose stimulation under convective (2 psi) (Conv) and diffusive transport (Diff) with subjection to cytokines (+Ck). Experiments with cytokine exposure (+Ck) consisted of media containing TNF-α (2000 U/mL), IFN-γ (1000 U/mL), and IL-1β (10 000 U/mL). The naked islets cultured under static conditions served as controls (Control, + Ck). The SNM- and SμM-encapsulated islets under convective transport (SNM, Conv, + Ck & SμM, Conv, + Ck) exhibited higher insulin secretion following stimulation at high glucose concentration and faster insulin release kinetics in response compared to those under diffusive transport (SNM, Diff, + Ck) and naked islets cultured under static conditions (Control, + Ck) (mean ± SEM, $n \geq 3$). (b) Stimulation index (SI) calculated as the ratio of (1) the first insulin collection in the high glucose phase at 40 min to the last insulin collection point of the previous low glucose phase at 30 min (Immediate Stimulation), and (2) the highest insulin secretion in the high glucose phase to the last insulin collection point of the previous low glucose phase at 30 min (Maximum Stimulation). The SI indicates the magnitude of insulin released as stimulated by a higher concentration of glucose. With cytokine exposure (+Ck), SμM-encapsulated islets under convective transport (SμM, Conv) showed the highest magnitude in glucose-induced

insulin secretion compared to other conditions (Immediate Stimulation). However, when using the highest insulin secretion in the high glucose phase (Maximum Stimulation), the calculated SI was the highest for SNM-and SμM-encapsulated islets under convection (SNM, Conv & SμM, Conv) compared to that under diffusion (SNM, Diff) and naked islets cultured under static conditions (Control) (mean ± SEM, $n \geq 3$, $^{*}p < 0.05$). (c) Shut-down index (SDI) calculated as the ratio of (1) the first insulin collection point in the subsequent low glucose phase at 70 min to the last insulin collection point in the high glucose phase at 60 min (Immediate Shutdown), and (2) the lowest insulin secretion in the subsequent low glucose phase to the last insulin collection point in the high glucose phase at 60 min (Maximum Shutdown). The SDI reflects the magnitude of cessation in insulin production once glucose concentration returns to normal. With cytokine exposure (+Ck), the SNM- and SμM-encapsulated islets under convection (SNM, Conv & SμM, Conv) exhibited the highest magnitude of insulin reduction compared to the diffusive condition (SNM, Diff) and the naked islet culture (Control) as glucose dropped low (Immediate Shutdown & Maximum Shutdown) (mean ± SEM, $n \geq 3$, $^{*}p < 0.05$).

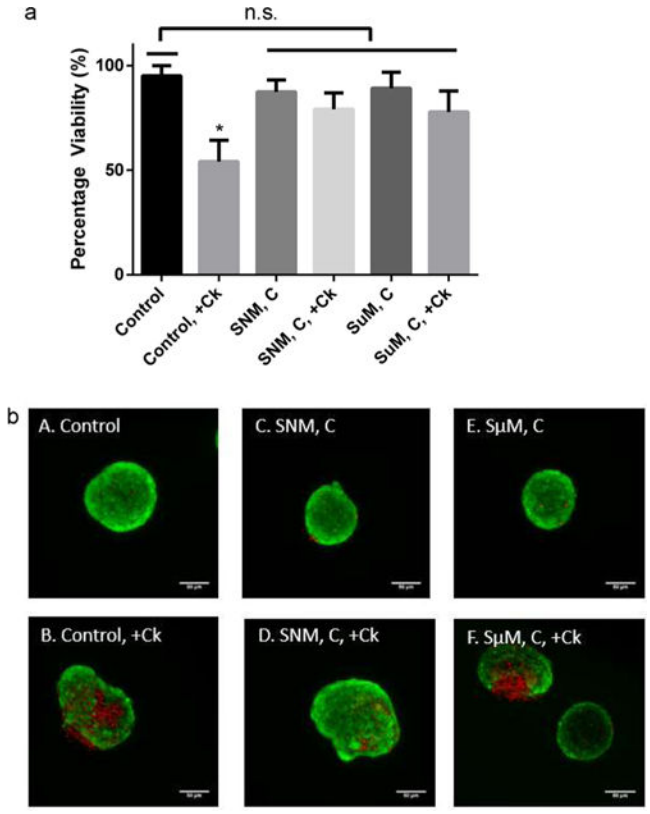

Figure 4.

In vitro viability of mouse islets. (a) Viability of mouse islets was measured following the 90 min low−high−low (1.6, 16.6, and 1.6 mM) glucose stimulation in which islets were subjected to the mock-loop circuit with (+Ck) or without cytokine exposure for SNM- and SμM-encapsulation under convection (SNM, C & SμM, C). The naked islet culture under static culture with cytokine exposure (Control,+Ck) showed significantly less viability compared to all other conditions (mean ± SEM, $n \geq 3$, $^*p < 0.05$). (b) Viable (green) and dead (red) cells were stained for control static culture without cytokines (A: Control), control static culture with cytokines (B: Control, + Ck), SNM-encapsulated mouse islets under convection without cytokines (C: SNM, C), SNM-encapsulated mouse islets under convection with cytokines (D: SNM, C, + Ck), SμM-encapsulated mouse islets under convection without cytokines (E: SμM, C), and SμM-encapsulated mouse islets under convection with cytokines (F: SμM, C,+Ck). Experiments with cytokine exposure (indicated by+Ck) consisted of media containing TNF-α, IFN-γ, and IL-1β. Both control static culture with cytokines (B: Control, + Ck) and SμM-encapsulated mouse islets under convection with cytokines (F: SμM, C, + Ck) showed a higher level of islet damage compared to other groups, however, the viability of SμM-encapsulated mouse islets under convection with cytokines (F: SμM, C, + Ck) was not statistically significant (n.s.).

Table 1

Rate of Change in Insulin Secretion without Cytokine Exposure[a]

experimental condition	low—high glucose stimulation (× 10^{-2}) (normalized insulin content min^{-1})	high—low glucose shut- down (× 10^{-2}) (normalized insulin content min^{-1})
Control	0.86	−0.71
SNM, Diff	0.84	−0.42
SNM, Conv	1	−2.71
SμM, Conv	3.15	−3.36

[a]The rate of change in insulin production was calculated based on the slopes of curves that were fitted on glucose—insulin kinetics graphs to describe the quickness of insulin being secreted as glucose concentration changes. Without subjection to cytokines, SμM-encapsulated mouse islets under convection (SμM, Conv) showed the fastest response following high glucose exposure, whereas SNM- and SμM-encapsulated mouse islets under convection (SNM, Conv & SμM, Conv) exhibited a similar rate of insulin cessation when glucose concentration returned to normal.

Table 2

Rate of Change in Insulin Secretion with Cytokine Exposure[a]

experimental condition	low–high glucose stimulation (× 10^{-2}) (normalized insulin content min^{-1})	high–low glucose shut- down (× 10^{-2}) (normalized insulin content min^{-1})
Control, + Ck	0.22	−0.092
SNM, Diff, + Ck	0.73	−0.32
SNM, Conv, + Ck	2.89	−1.76
SμM, Conv, + Ck	1.57	−2.84

[a]The rate of change in insulin production was calculated on the basis of the slopes of curves that were fitted on glucose—insulin kinetics graphs to describe the quickness of insulin being secreted as glucose concentration changes. With subjection to cytokines (+Ck), SNM-encapsulated mouse islets under convection (SNM, Conv) showed the fastest response following high glucose exposure while SNM- and SμM-encapsulated mouse islets under convection (SNM, Conv & SμM, Conv) exhibited similar rate of insulin cessation when glucose concentration returned to normal.